J Mol Model (2014) 20:2489
DOI 10.1007/s00894-014-2489-9

ORIGINAL PAPER

Computational study on the effects of substituent and heteroatom on physical properties and solar cell performance in donor-acceptor conjugated polymers based on benzodithiophene

Lvyong Zhang · Wei Shen · Rongxing He · Xiaorui Liu · Zhiyong Fu · Ming Li

Received: 16 August 2014 / Accepted: 6 October 2014 / Published online: 22 October 2014

Abstract Computationally driven material design has attracted increasing interest to accelerate the search for optimal conjugated donor materials in bulk heterojunction organic solar cells. A series of novel copolymers containing benzo[1,2-b:4,5-b']dithiophene (BDT) and thieno[3,4-c]pyrrole-4,6-dione (TPD) derivatives were simulated by density functional theory (DFT) and time-dependent density functional theory (TD-DFT). We performed a systematic study on the influences on molecular geometry parameters, electronic properties, optical properties, photovoltaic performances, and intermolecular stacking as well as hole mobility when different chalcogenophenes in TPD derivatives were used and functional groups with different electron-withdrawing abilities such as alkyl, fluorine, sufonyl, and cyano were introduced to the nitrogen positions in electron-deficient units. The substitution position of electron-withdrawing groups may cause little steric hindrance to the neighboring donor units, especially fluorine and cyano group. It was found that the incorporation of these new electron-deficient substituents and sulfur-selenium exchange can be applicable to further modify and optimize existing molecular structures. Our findings will provide valuable guidance and chemical methodologies for a judicious material design of conjugated polymers for solar cell applications with desirable photovoltaic characteristics.

Keywords Benzo[1,2-b:4,5-b']dithiophene · Chalcogenophenes · Electron-withdrawing groups · Organic solar cell · Thieno[3,4-c]pyrrole-4,6-dione

Introduction

In the past few years, organic solar cells, especially the bulk heterojunction polymer solar cells have attracted much attention because of their advantages of low cost, easy fabrication, light weight, and the capability to fabricate flexible large-area devices [1]. The development of new device architectures including tandem and ternary solar cells has enabled organic polymer solar cells to break through the benchmarking efficiency of 10 % [2–4]. However, the current challenges for organic solar cells are still to improve the power conversion efficiency (PCE) as well as durability and costeffectiveness, to compete with their silicon-based counterparts [2].

When a light irradiates the active layer of the organic solar cells through the transparent indium tin oxide electrode, the conjugated polymer donor will absorb photons to produce electron–hole pairs which will diffuse toward the donor/acceptor interface where the electrons will transfer from the LUMO of the donor to the LUMO of the acceptor [3]. In the meantime, the holes have a similar process of electrons. Then the separated electrons and holes will be collected by metal cathode and indium tin oxide anode after a transport along acceptor and conjugated polymer interpenetrating network to form photocurrent and photovoltage. The design and synthesis of new conjugated donor materials with desirable chemical and physical properties was very important in realizing highly efficient organic solar cells, along with effective control of

Electronic supplementary material The online version of this article (doi:10.1007/s00894-014-2489-9) contains supplementary material, which is available to authorized users.

L. Zhang · W. Shen · R. He · X. Liu · Z. Fu · M. Li (✉)
School of Chemistry and Chemical Engineering, Southwest University, Chongqing 400715, People's Republic of China
e-mail: liming@swu.edu.cn

L. Zhang
e-mail: zhyong2013@swu.edu.cn

charge generation, separation, transport, and extraction [5–7]. A general strategy to design p-type conjugated polymer is a donor-acceptor alternating polymer structure [4], which leads to a low band gap for efficient light harvesting.

Recently, the photovoltaic performances of alternating copolymers containing benzo[1,2-b:4,5-b']dithiophene (BDT) as the donating moiety have attracted much attention, because it possesses a planar structure and BDT-containing copolymers have high hole mobility and suitable electronic energy levels [5, 8]. Some BDT-based small molecules and polymers show great potential in organic solar cells with high PCEs up to 8 % with high open-cicuit voltage (V_{oc}) [9–11]. Thieno[3,4-c]pyrrole-4,6-dione (TPD) unit [6, 7] with relatively simple, compact, symmetric, and planar structure could be beneficial for electron delocalization when it is incorporated into various conjugated polymers. The chemical structure of BDT segment and TPD fragment is illustrated in Scheme 1. Zou and coworkers have designed, synthesized, and characterized a new copolymer combining BDT and TPD units with a resulting PCE reached 5.5 % [12]. However, the relatively weak electron-withdrawing ability of TPD unit may be the main factor limiting the polymer solar cell performance [13]. Herein, to maximize the overall performance of organic polymer solar cells, further structural modifications to the electron-deficient unit are undoubtedly necessary.

Computationally driven material design has attracted increasing interest [9, 14], many quantum mechanical simulations on the polymer systems have focused on the influence of substituent on the performance of polymer solar cells, including TPD-based push-pull conjugated polymers [15–18]. However, a study of electron-withdrawing group on nitrogen atom with little steric hindrance between neighboring aromatic repeat units in BDT-TPD-based copolymers appears to be lacking, which can be a useful method for enhancing intramolecular electron transfer in donor-acceptor conjugated polymers. In this study, theoretical analysis on the influences of substitution group with different electron-withdrawing ability like alkyl, sulfonyl, fluorine, and cyano groups on the interesting position on photophysical properties of the copolymer, as well as heteroatom effects of chalcogen substitutions into the thiophene units of TPD derivatives, is reported. The chemical structure of studied conjugated polymers is depicted in Scheme 1. Through a series of structural modifications to the electron-deficient unit, we aim to provide insightful strategy and chemical methodologies to the future rational design of conjugated donor materials, especially to meet the particular requirements of different device architectures on the donor components, such as a prominent photocurrent or photovoltage combined with a high efficiency, to further maximize the overall performance of polymer solar cells.

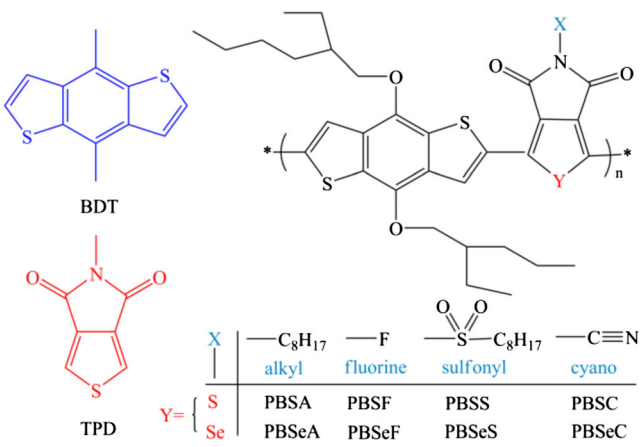

Scheme 1 Chemical structure of BDT segment, TPD fragment, and studied conjugated polymers. The polymers are named at the bottom according to the variety of the heteroatom and substitution group

Computational details

Geometry optimizations and simulation of optical absorption spectra were performed by DFT and TD-DFT, as implemented in the Gaussian09 program suite [10]. The side chain alkyl of copolymers merely aided in improving solubility without affecting electronic and optical properties [11], to simplify the calculation, all alkyl branched-chains were replaced by ethyl groups, and the terminals of the repeating units were saturated with hydrogen atoms. In order to find an appropriate functional and basis set for the calculations of studied polymers, we choose three hybrid functionals including PBE0 [19], PBEh1PBE [20], and mPW1PBE [19] at 6-31G* and 6-311G* basis sets to calculate the dimer models of PBSA and PBSeA. As shown in Table S1 and Table S2, the calculated results of HOMO energy levels at mPW1PBE/6-31G* level (−5.50 and −5.48 eV for DBSA and DBSeA, respectively; here "D" means dimer) agree well with the experimental values of the polymers (−5.56 and −5.51 eV for PBSA and PBSeA, respectively) [21]. Thus, the ground state geometries of all dimers and monomers were optimized in gas-phase within the mPW1PBE functional, using 6-31G* basis set, meanwhile the HOMO energy levels of dimers were predicted. To predict the band gaps (vertical exCitation energy) of these polymers, three kinds of time-dependent density functional methods of mPW1PBE [19], B3LYP [22], and O3LYP [23] with different basis sets were applied both in gas phase and in chloroform solution. As listed in Table S3-S6, all vertical electronic transition energy of the first excited states (S1) and oscillator strength (f) are smaller in gas phase than in chloroform solution, but the energy gaps and f of the second exited states (S2) are almost unchanged. Among those methods, the TD-O3LYP/6-311G* approach in chloroform solution (2.08 and 2.04 eV for DBSA and DBSeA, respectively) is the best choice to save computational time and in agreement with the experimental values (2.03 and

1.95 eV for PBSA and PBSeA, respectively) [21]. Moving to the direct comparison of normalized experimental absorption spectra and calculated spectra at O3LYP/6-311G* level in chloroform solution for PBSA and PBSeA, reported in Fig. 1, we can see our simulations well reproduce the experimental results with slightly blue shift, within 0.1 eV. Therefore, we conducted the following band gap calculations and discussions using the same method with a dimer model. The LUMO energy levels were estimated from the equation [24], $E_{LUMO}=E_{HOMO}+E_{g,TD}$. A similar strategy has been used in the experiments ($E_{LUMO}=E_{HOMO}+E_{opt}$) [15]. There are no imaginary frequencies for all monomers and dimers at the present theoretical level. It implies that all the optimized structures are the global minima on the potential energy surface and stable structures.

Electronic density topological analyses were carried out at the B3LYP/6-31G* level based on the optimized geometries. The topological analyses are obtained from the atom in molecule (AIM) calculation [16]. The natural bond orbital (NBO) [17] analysis is also carried out at the B3LYP/6-31G* level on the optimized geometries. In the computation of the reorganization energy, the cation geometry of molecules were also carried out at mPW1PBE/6-31G* level, and the energy of the neutral geometry based on the optimized cation geometry, was obtained from single point energy computation in the same method [18, 25]. The correlative computations of transfer integral are performed at PW91PW91/6-31G** level on dimers [26] and the π-stacking distance between the two adjacent segments was scanned by M062X/6-31G** [27].

Results and discussion

Geometry parameters and electronic properties

The geometry parameters and electronic properties of monomers involving MBSA, MBSeA, MBSF, MBSeF, MBSS, MBSeS, MBSC, and MBSeC (here "M" means monomer), as well as intramolecular charge transfer (D_{CT}) based on optimized structures, are shown in Fig. 2. Inspected Fig. 2, it can be seen that the dihedral angles in studied monomers are in close proximity to 0°. So these compounds all are coplanar structures. The sum of natural charges (S_{NC}) is positive in BDT units and negative in TPD derivatives. It indicates that the charges are partly transferred from BDT units to TPD derivatives in these monomers. The amount of intramolecular charge transfer (D_{CT}) which is defined as the absolute value of S_{NC} could be used to exhibit the electron-withdrawing power of molecular segment. The D_{CT} in MBSA, MBSeA, MBSF, MBSeF, MBSS, MBSeS, MBSC, and MBSeC are 0.058, 0.054, 0.079, 0.074, 0.078, 0.075, 0.097, and 0.093, respectively. It indicates the thiophene-based (S series) molecules give stronger electron withdrawing ability than selenophene-based (Se series) molecules. In S series (a similar trend in Se series), the sequences of the values of D_{CT} are MBSC>MBSF>MBSS>MBSA, while the electron-withdrawing abilities of the substituents are in the order of MBSC>MBSS>MBSF>MBSA. It indicates the sequence of MBSS and MBSF is abnormal, which may be caused by the steric hindrance of sulfonyl group between neighboring thiophene unit. However, more atomic interactions exist in sulfonyl-based compounds, like O_2 to O_4 and O_1 to H_1, which play a major role in the electronic properties and molecular stability of these monomers. Compared the bond length of carbon-chalcogen (C_2-Y), C_2=C_3 and C_3-C_4 in S series molecules with that in Se series molecules, taking MBSA and MBSeA as examples, it can be seen that the bond length of C_2-Se (1.886 Å) for MBSeA is longer than C_2-S (1.758 Å) for MBSA due to the different sizes of sulfur and selenium, while the C_2=C_3 double bond length (1.374 Å) for MBSeA is slightly shorter than that for MBSA (1.376 Å) and C_3-C_4 single bond length (1.423 Å) for MBSeA is slightly longer than that for MBSA (1.419 Å).

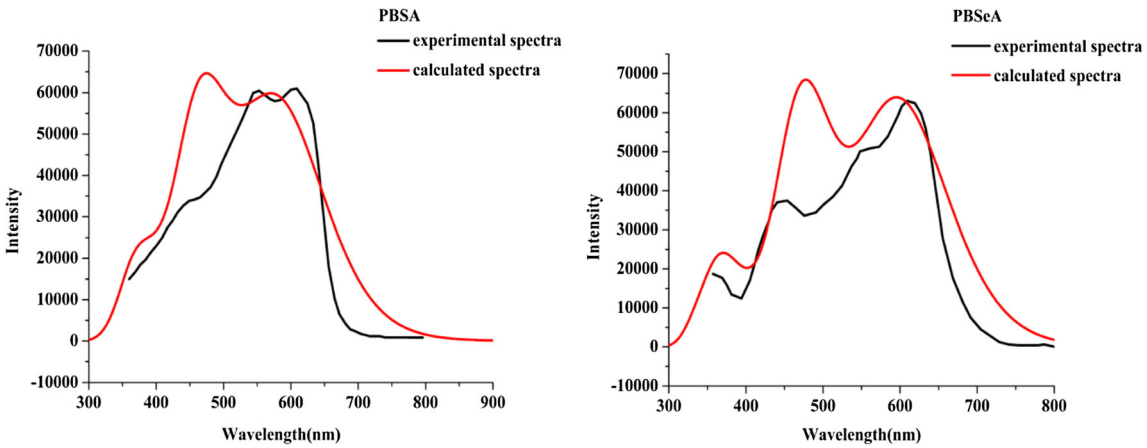

Fig. 1 Comparison between the normalized experimental (black line) and calculated absorption spectra (red line) in chloroform solution by O3LYP/6-311G* for PBSA (left) and PBSeA (right)

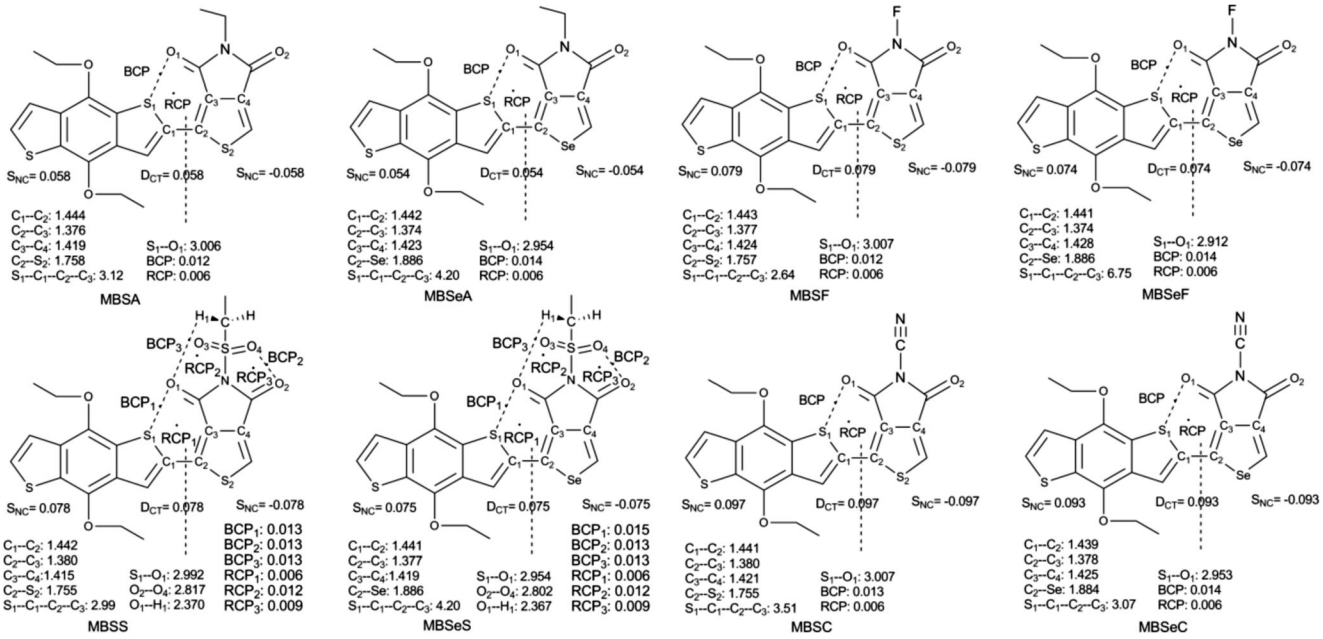

Fig. 2 Geometry parameters and electronic properties of all studied monomers

In order to obtain detailed bonding character, the completely topological analyses are performed for the central bonds (C_1-C_2) of all studied monomers. The bonding critical points (BCPs) are points of minimum electron density ρ(r) along the bond [16]. It provides a measure for the π character of a bond and structural stability. The charge densities ρ(r), the Laplacian $\nabla^2_\rho(r)$, the Wiberg bond indexes (WBIs) [28] as well as the bond length (L_B) are listed in Table 1. Inspecting Table 1, we can find that the bond lengths of central bond (in the range of 1.439-1.444 Å) are larger than that of C = C (1.33 Å) and smaller than that of C-C (1.54 Å). In view of S series molecules, it can be easily found that the order of the bond lengths of central bond is MBSA>MBSF>MBSS>MBSC by examining individual compound. In the meantime, the bond lengths of the Se molecules are smaller than that of the corresponding S molecules. This trend is tightly related to the electron-withdrawing capacity of electron-deficient units. The electron-withdrawing power of S series molecules (a similar trend in Se series) are sorted in the order of MBSC>MBSS>MBSF>MBSA. These analyses indicate that the electron-withdrawing power of TPD derivatives in push-pull conjugated compounds has an impact on the structures. In S series molecules, both electronic density ρ(r) (more positive) and Laplacian $\nabla^2_\rho(r)$ (more negative) of central bonds increase with the electron-withdrawing ability of the substitutions. The ε_{BCP} and WBIs are also increased upon electron-withdrawing power of the substitutions, which suggest that the π characters of the central bonds are strengthened. It can also show that there is the same trend from S molecules to Se molecules which indicate the substitution of sulfur by selenium also strengthen the π character. When it comes to Se series molecules, this trend is changed between MBSeS and MBSeF, which implies that synergistically incorporating selenium and fluorine may be a useful approach to enhancing effective π-conjugation.

Table 1 BCP properties of central bond in monomers

Monomers	ρ(r)	$\nabla^2_\rho(r)$	ε_{BCP}	L_B(Å)	WBIs
MBSA	0.2827	−0.7195	0.134	1.444	1.140
MBSF	0.2832	−0.7220	0.136	1.443	1.144
MBSS	0.2833	−0.7222	0.137	1.442	1.147
MBSC	0.2856	−0.7329	0.144	1.441	1.151
MBSeA	0.2835	−0.7216	0.126	1.442	1.150
MBSeF	0.2840	−0.7243	0.128	1.441	1.154
MBSeS	0.2839	−0.7231	0.129	1.441	1.156
MBSeC	0.2847	−0.7268	0.131	1.439	1.161

After analysis of these results, it is clear that the changes of substituted functional group and heteroatom have an impact on the whole molecular geometry and electron properties. Both the strengthening of substituent electron-withdrawing power and substituting sulfur in these TPD-bassed structures with selenium could contribute to effective π-conjugation and enhance the stability of the whole system. The geometric and electronic differences may undoubtedly create the changes of other properties.

Optical properties

The vertical singlet-singlet electronic transition energies and optical absorption spectra of all polymers were calculated at O3LYP/6-311G* level in chloroform solution with a dimer model Fig. 3 shows the simulated absorption spectra

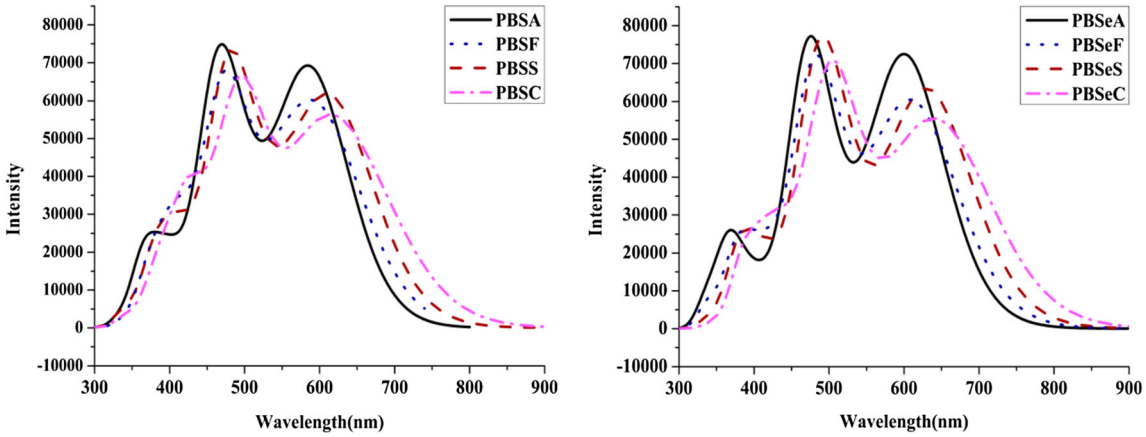

Fig. 3 Calculated optical absorption spectra of S series molecules (left) and Se series molecules (right)

(considering the first 20 excited states). The calculated electronic transitions, oscillator strength (f), and main configurations of all dimers are listed in Table 2.

The main transitions of all donors in visible range correspond to the transitions from HOMO to LUMO, HOMO to LUMO+1, HOMO to LUMO+2, HOMO-1 to LUMO, and HOMO-2 to LUMO. As shown in Table 2 and Fig. 3, the maximum absorbent wavelengths of DBSA, DBSF, DBSS, and DBSC are 597, 625, 631, and 671 nm, respectively; indicating S series are red-shifted with the increase of the substituent electron-withdrawing ability. In the meantime, a similar tendency for predicted maximum absorption wavelengths of Se series could be found. Compared with S series molecules, the calculated S_0 to S_1 absorptions of DBSeA, DBSeF, DBSeS and DBSeC are 609, 634, 643, and 681 nm, respectively, which indicated that the first absorption peaks of

Table 2 Calculated electronic transitions, oscillator strength (f) and main configurations of all dimers

dimers		E^{ex} (eV)	λ_{max} (nm)	f	Major configuration	Exp.λ (nm)
DBSA	S_1	2.08	597	0.75	H→L(98 %)	610[a]
	S_2	2.34	554	0.28	H-1→L(93 %), H→L+1(4 %)	550[a]
	S_5	2.67	465	0.76	H-2→L(92 %), H→L+2 (7 %)	
DBSF	S_1	1.98	625	0.44	H→L(98 %)	
	S_2	2.16	575	0.45	H-1→L(93 %), H→L+1(4 %)	
	S_6	2.62	474	0.80	H-2→L(90 %), H→L+2 (6 %)	
DBSS	S_1	1.97	631	0.59	H→L(98 %)	
	S_2	2.12	585	0.30	H-1→L (93 %),H→L+1 (4 %)	
	S_6	2.59	478	0.65	H-2→L (62 %), H→L+2 (34 %)	
DBSC	S_1	1.85	671	0.34	H→L(98 %)	
	S_2	2.04	608	0.48	H-1→L(94 %), H→L+1(3 %)	
	S_6	2.50	496	0.72	H-2→L(87 %), H-1→L+2(7 %), H→L+2(4 %)	
DBSeA	S_1	2.04	609	0.83	H→L(98 %)	635[a]
	S_2	2.19	566	0.23	H-1→L(94 %), H→L+1(3 %)	565[a]
	S_5	2.63	472	0.84	H-2→L (96 %)	
DBSeF	S_1	1.96	634	0.53	H→L(98 %)	
	S_2	2.12	585	0.39	H-1→L(95 %), H→L+1 (3 %)	
	S_5	2.57	482	0.53	H-2→L (66 %), H→L+2 (31 %)	
DBSeS	S_1	1.93	643	0.68	H→L(98 %)	
	S_2	2.07	599	0.24	H-1→L(95 %), H→L+1 (3 %)	
	S_5	2.54	489	0.84	H-2→L (92 %), H→L+2 (5 %)	
DBSeC	S_1	1.82	681	0.41	H→L(98 %)	
	S_2	2.00	620	0.45	H-1→L(95 %), H→L+1 (2 %)	
	S_6	2.48	501	0.55	H-2→L(61 %), H→L+2 (34 %)	

[a] from reference [21]

the studied molecules are red-shifted from S series to Se series due to the strengthened conjugated effect (see section Geometry parameters and electronic properties). Hence, compared to the initial structure, the absorption peaks of modified molecules become much broader, which will facilitate more efficient sunlight absorption.

For an in-depth research of electron transition, the electron density difference plots of electronic transitions for the main excited states of all dimers are illustrated in Fig. 4. As shown in Table 2 and Fig. 4, three obvious absorption peaks of all these dimers are assigned to $\pi \rightarrow \pi^*$ type transitions. The S_0 to S_1 absorption peaks of all dimers are assigned to electron transfer from HOMO to LUMO correspond to intramolecular electron transfer direction substantially from the electron-rich units to the electron-withdrawing units. The second absorption transitions of all calculated dimers correspond to HOMO-1 to LUMO and HOMO to LUMO+1, showing more obvious separations of electrons and holes. When it comes to the third transitions with the largest absorption intensity, the transitions of almost all dimer models are assigned to HOMO-2 to LUMO and HOMO to LUMO+2, showing the most complete charge separation. It is thus clear that our structural modifications make little difference to the transitions above and that all absorption wavelengths are corresponding to obvious electronic transitions which implies that all molecules would have favorable absorption capacity in both visible region and near-infrared region.

Photovoltaic properties

Frontier molecular orbital surfaces play a major role in explaining the changes of energy level with our molecular modifications. We plotted the contour plots of HOMO and LUMO orbitals of all dimers in Fig. 5. Figure 5 shows that the HOMOs of all the molecules are spread over the whole π-conjugated backbones and display anti-bonding character between two adjacent fragments and bonding character within each unit. Therefore, the structural changes (by incorporating different electron-withdrawing groups and sulfur-selenium exchange) on the acceptor units will contribute to the LUMOs of the donor-acceptor units in the same way as to the LUMOs of separated acceptor units. In the case of LUMOs, electrons are withdrawn from the ring junctions and localized on the accepter moieties. The LUMOs of these push-pull polymers arise from the bonding linear combination from the lowest unoccupied orbitals of the corresponding acceptor units with the right symmetry and the LUMOs of the corresponding donor units. As a result, our structural modifications have an impact on the LUMOs of whole molecules. Moreover, the HOMOs and LUMOs topologies show certain overlap, which is a prerequisite to allow for an effective intramolecular charge transfer.

It is interesting to analyze the effect of structural modifications on photovoltaic properties of the resulting molecules. The band gap of the polymer should be minimized to maximize the spectral absorption and thereby achieving better

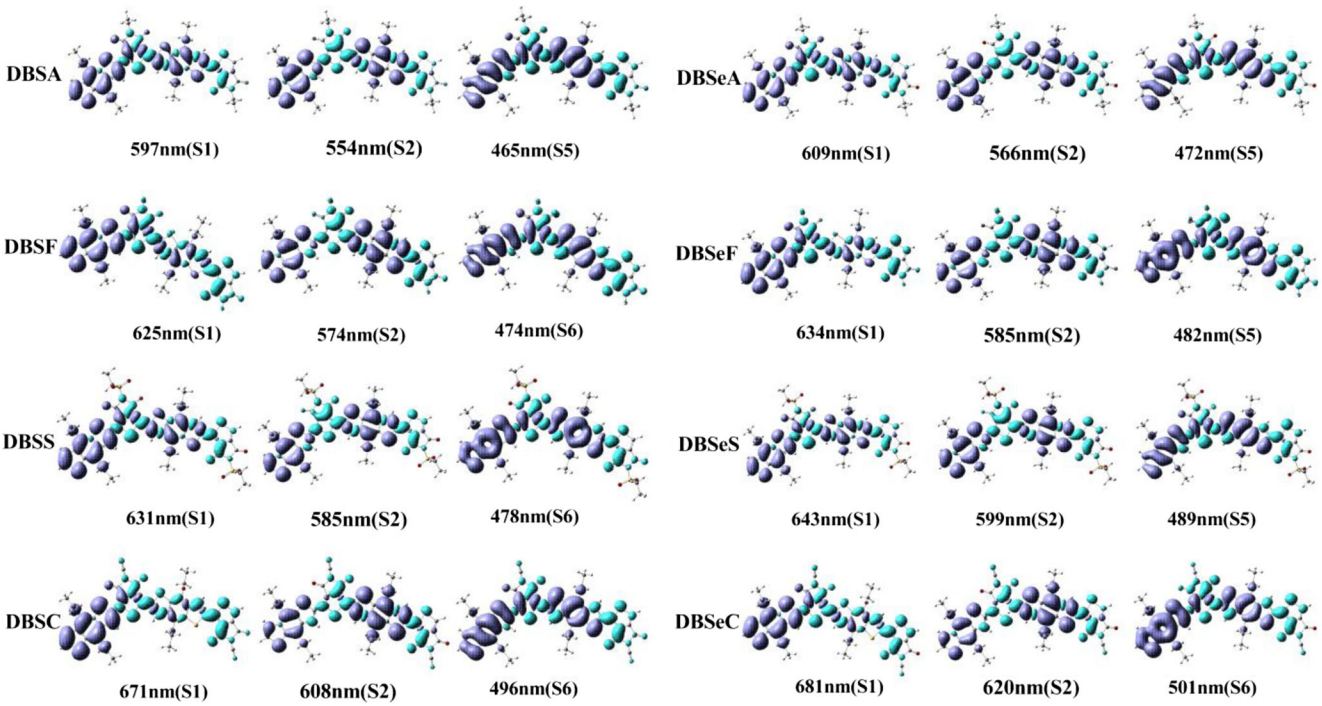

Fig. 4 Electron density difference plots of transitions for the main excited states of S series (left) and Se series (right). Blue and purple colors correspond to an increase and decrease of electron density, respectively

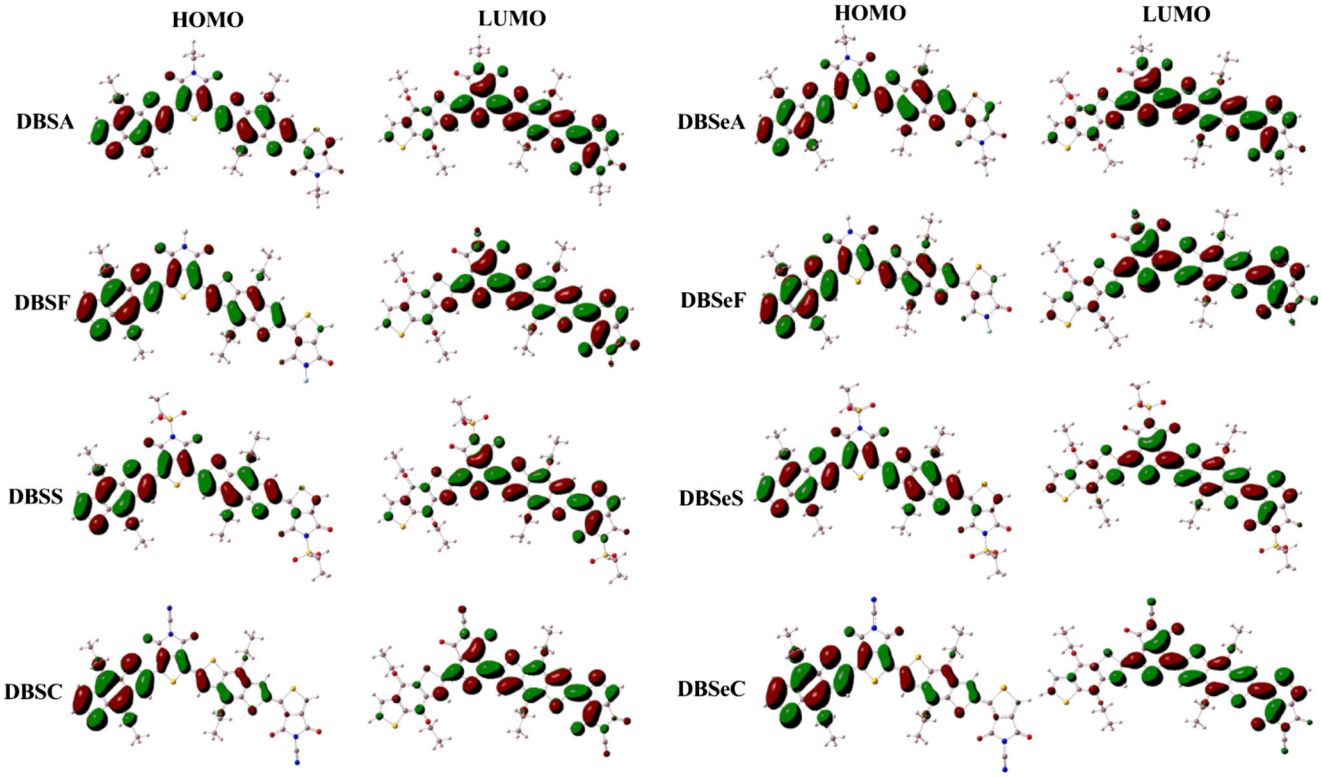

Fig. 5 The contour plots of frontier molecular orbital for all D-A dimer models

performance. With smaller energy gap, it can obtain absorption in the infrared and near-infrared (NIR) regions, where the maximal photon flux of the sun is located [29]. In the meantime, to obtain efficient charge transfer to the acceptor, donor must posses a downhill energetic driving force which exceeds the binding energy. The binding energy from the coulomb interaction in the donor is estimated to be 0.2~1.0 eV [30]. The photovoltaic parameters of all studied molecules are listed in Fig. 6

As shown in Fig. 6, for the S molecules and their corresponding Se molecules, the values of HOMO energy levels follow the order DBSC<DBSF<DBSS<DBSA, which agrees with the values of D_{CT}. The values of LUMO

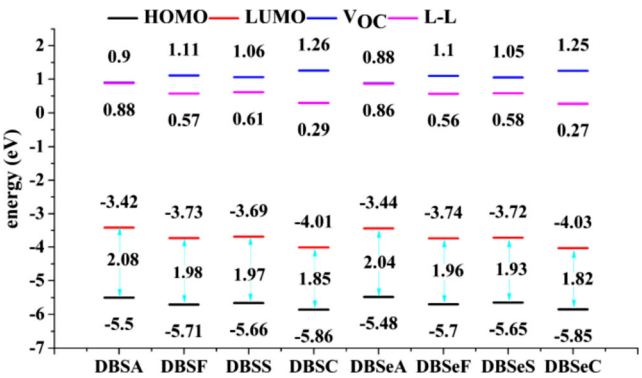

Fig. 6 Photovoltaic parameters of all studied molecules

levels follow the same trend with the values of HOMO levels. However, the band gaps follow a different trend, that is, DBSC<DBSS<DBSF<DBSA. The reason for the difference may be that the fluorine on DBSF (DBSeF) is less conjugated with the backbone than sulfonyl group on DBSS (DBSeS). It obviously shows that DBSC (DBSeC) has the lowest energy gap due to the strong inductive and conjugative effect of cyano group. On the other hand, from S molecules to Se molecules, the values of HOMO levels are increased by 0.1 eV, which may be caused by a slightly weaker electronegativity of selenium than that of sulfur. However, there is a reduced tendency for the LUMO levels with this sulfur-selenium exchange, which contributes to a smaller energy gap. These findings verify the conclusions in the reported works [31] and confirm that changing the electron withdrawing ability of substituted functional groups on nitrogen atoms of TPD-based conjugated polymers and thiophene-selenophene exchange in TPD derivatives can be an effective tool to tune their molecular energy levels.

Another key parameter of bulk heterojunction polymer solar cells is the open circuit voltage (V_{OC}) [32]. It is well known that the larger the V_{OC} value is, the better the performance of solar cells will be [33]. In this contribution, the HOMO (D)-LUMO (A) offset model was adopted in consideration of the fact that the work function difference between indium tin oxide and Al electrode is outside the range −3 and

0 eV [34]. So the V_{OC} of the polymer-$PC_{61}BM$ solar cell can be estimated as Eq. (1) [35]:

$$V_{OC} = \frac{1}{e}\left(\left|E^{D}HOMO\right| - \left|E^{A}LUMO\right|\right) - 0.3\ V, \quad (1)$$

where e represents the elementary charge and the value of 0.3 V is an empirical factor. $E^{A}LUMO$ is equivalent to −4.3 eV. In order to obtain high V_{OC}, the lower HOMO level is required as the p-type materials in organic solar cells. In Fig. 6, the calculated V_{OC} of DBSA, DBSF, DBSS, and DBSC are 0.90, 1.11, 1.06, and 1.26 eV, respectively. These values are sorted in the order of DBSC>DBSF>DBSS>DBSA, which agree well with the values of HOMO energy levels. It obviously shows cyano-contained compounds have the greatest V_{OC} due to the strongest electron-withdrawing ability of cyano group. The same as S series molecules, the V_{OC} of Se molecules follow the order DBSeC>DBSeF>DBSeS>DBSeA.

According to the design criteria, to obtain efficient charge transfer to the acceptor, donor must possess a downhill energetic driving force which should exceed the binding energy. The binding energy from the Coulomb interaction in the donor is estimated to be 0.2~1.0 eV [36]. Empirically, the energetic driving force for charge transfer from the donor to the acceptor is represented by the energy difference between the LUMO levels of donor and acceptor. However, an energy difference that is too much larger may result in a waste of energy, accounting for that it does not contribute to the device performance. As shown in Fig. 6, in view of S and Se molecules, the downhill energetic driving forces are all beyond the binding energy according to the L-L values. However, an energy difference that is too much may result in a waste of energy. It also shows that our molecular modifications are effective ways to reduce the L-L values to make better use of energy. And above all, these ways of energy level modulation is strongly dependent on the material structure and the energy level matching in different contexts [37, 38], but the trend with structural modifications may be very insightful in designing new materials.

Hole transport properties

In the organic solar cells, high hole mobility for the donors as a hole transport layer is helpful to enhance the charge transport efficiency of the devices [8]. Currently, there are two types of models to describe the carrier draft in materials (the coherent band model and the hoping model) [39, 40]. At very low temperature, the charge transport in materials can be described by a bandlike regime. At room temperature, it is generally accepted that the carrier transport in materials can be described as carrier hoping between neighboring molecules by hoping model. According to Marcus-Hush theory [41, 42], the carrier transport for organic materials can be described by a hoping mechanism.

The hole mobility is evaluated from the Einstein relation [43, 44],

$$\mu = \frac{eD}{K_B T}\ . \quad (2)$$

Here e, D, K_B, and T stand for the electron charge, the charge diffusion coefficient, Boltzmann constant, and temperature, respectively. Ford-dimensional system,

$$D = \lim_{t\to\infty}\frac{1}{2d}\frac{\left\langle x(t)^2\right\rangle}{t} \approx \frac{1}{2d}\sum_i r_i^2 k_i p_i\ . \quad (3)$$

where d is the spatial dimensionality, i runs overall nearest adjacent molecules and r_i, k_i,and p_i are the corresponding π-stacking distance, charge transfer rate, and hopping probability, respectively. Furthermore, when considering about only one neighbor, the diffusion constant along a single molecular dimer is simply defined as [45, 46]:

$$D = \frac{1}{2}kr^2, \quad (4)$$

where k and r are the charge transfer rate and intermolecular distance for dimer, herein, the hole mobility is expressed as [43, 44]:

$$\mu = \frac{er^2}{2K_B T}k\ . \quad (5)$$

The widely used charge transfer rate from the classical Marcus theory reads [47]:

$$k = \frac{t^2}{\hbar}\sqrt{\frac{\pi}{\lambda k_B T}}\exp\left(-\frac{\left(\lambda + \Delta G^0\right)^2}{4\lambda k_B T}\right). \quad (6)$$

Here t is the transfer integral between the initial and final states, λ is the reorganization energy which is defined as the energy change associated with the geometry relaxation during the charge transfer, and ΔG^0 is the relevant change of total Gibbs free energy. Since the studied molecular semiconductors contain only one kind of molecule, the charge transfer in an adjacent molecular dimer is a self-exchange reaction process. Therefore, ΔG^0 equals zero and Eq. (5) then becomes

$$k = \frac{t^2}{\hbar}\sqrt{\frac{\pi}{\lambda k_B T}}\exp\left(-\frac{\lambda^2}{4\lambda k_B T}\right). \quad (7)$$

It is clear that the two key parameters are the reorganization energy and transfer integral. The reorganization energy λ is composed of two parts [48]: inner reorganization energy λ_i and outer reorganization energy λ_o. In the case of solar cells, which are condensed-state systems, the latter could be ignored, thus the former becomes dominant. The inner reorganization energy λ_i could be calculated as follows:

$$\lambda = \lambda_1 + \lambda_2 = E_+ - E_+^* + E^* - E\,. \tag{8}$$

Here we use E and E_+^* to stand for the energies of the neutral segment and the cation segment, respectively. Both of them lie in the lowest energy geometries, while E_+ and E^* denote the energies of the neutral segment and the cation segment with the geometries of the cation segment and the neutral segment, respectively [18, 25] the transfer integral t represents the electron coupling strength of the adjacent segments and can be estimated by Koopmans' theorem [49]. The transfer integral of hole are given by the following [50]:

$$t_h = \frac{1}{2}(E_H - E_{H-1}), \tag{9}$$

where E_H and E_{H-1} are the energies of the HOMO and HOMO-1 in the closed-shell configuration of the neutral state, respectively.

The transfer integral is directly connected with the carrier hopping pathways or intermolecular stacking. In this work, the two adjacent segments are stacked in the face-to-face direction. The π-stacking distance ($r_{\pi\text{-}\pi}$) is obtained from the lowest point of potential energy surface as shown in Fig. 7. The calculated reorganization energy (λ_h), π-stacking distance ($r_{\pi\text{-}\pi}$), transfer integral (t_h), hole transport rates (k_h), hole mobility (μ_h) of all dimers were listed in Table 3. As shown in Table 3, the introductions of the substituents have little influence on the values of λ_h except for sulfonyl-substituted compounds which have the highest λ_h (0.68 eV) which may be due to the largest changes in the geometry of sulfonyl-based dimer models when the electron transfer takes place. In the meantime, the π-stacking distance of sulfonyl-contained molecules is relatively high, especially the $r_{\pi\text{-}\pi}$ of DBSeA (0.46). Herein, this kind of molecules has relatively low mobility at last. On the other hand, there is an increasing tendency for the values of t_h with the strengthening of electron-withdrawing ability of the substituents, except for sulfonyl group. Along with the increase of electron-

Table 3 Reorganization energy (λ_h), π-stacking distance ($r_{\pi\text{-}\pi}$), transfer integral (t_h), hole transport rates (k_h), and hole mobility (μ_h) of all molecules. All the measure of energies is eV

Dimers	λ_h	$r_{\pi\text{-}\pi}$ (nm)	t_h	k_h	μ_h(cm^2V^{-1} s^{-1})
DBSA	0.50	0.40	0.03	1.64×10^{11}	5.12×10^{-3}
DBSS	0.68	0.40	0.03	2.45×10^{10}	7.62×10^{-4}
DBSF	0.51	0.38	0.04	2.63×10^{11}	7.38×10^{-3}
DBSC	0.51	0.38	0.06	5.91×10^{11}	1.66×10^{-2}
DBSeA	0.64	0.46	0.01	4.14×10^{9}	1.70×10^{-4}
DBSeS	0.68	0.38	0.04	4.35×10^{10}	1.22×10^{-3}
DBSeF	0.64	0.37	0.05	1.03×10^{11}	2.75×10^{-3}
DBSeC	0.62	0.38	0.06	1.84×10^{11}	5.16×10^{-3}

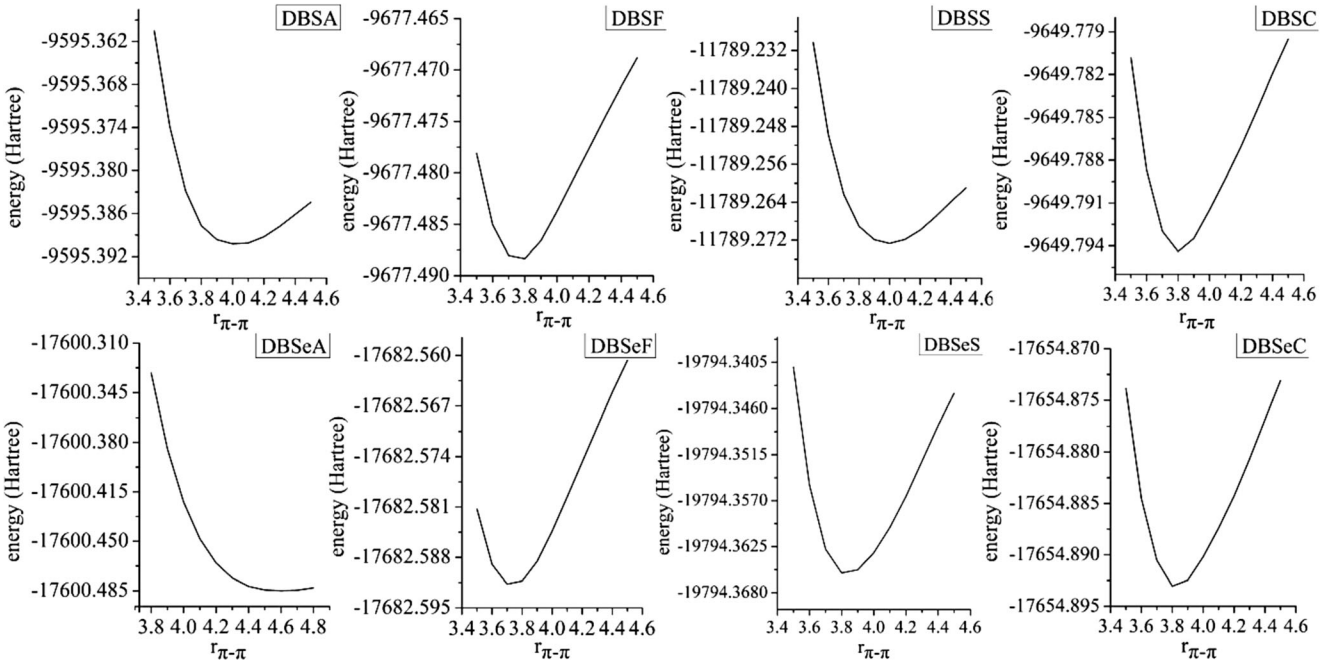

Fig. 7 Potential energy surfaces obtained by scan at M062X/6-31G** level

withdrawing power of functional groups, the mobility goes up due to the slightly vibrations of the values of λ_h and the lager t_h. It also shows that the incorporation of heavier atom (selenium) into thiophene of TPD derivative is disadvantageous to the hole mobility.

Conclusions

We report a comprehensive computational study of structural fine-tuning in relation to physical properties and solar cell performance for future design of conjugated donor polymers. A calibration study was carried out to test different functionals and check the basis set. Our results show the methods we used in this work could reproduce the experimental HOMO energy levels and optical band gaps of PBSA and PBSeA very well. We have performed a systematic study on the effects of alkyl, sulfonyl, fluorine, and cyano substitutions on nitrogen atoms of TPD derivatives by combination of heteroatom effects, aimed to get insight into the effects of structural modifications on the molecular structure, electron properties, optical properties, and photovoltaic properties as well as hole transport properties. The calculated results reveal that the incorporation of three substitution groups can not only obviously reduce the HOMO and LUMO level of molecules, but also enhance the light-absorbing efficiency and charge transport ability of polymers. Increasing the electron-withdrawing strength in D-A type donors is a rational way to improve the electronic, optical, and transport properties of the copolymers, therefore enhancing the performances of organic solar cells. On the other hand, substituting sulfur in original TPD-based structures with selenium can stabilize the whole molecule system and reduce the energy gap, although it has a slight impact on hole mobility. Hence, sulfur-selenium exchange is also an effective way to modify and optimize some molecular structures. This work will provide valuable guidance and chemical methodologies for material design of push-pull copolymers with desirable photovoltaic characteristics.

Acknowledgments This work was supported by National Natural Science Foundation of China (Grant No.2173144), and by Fundamental Research Funds for the Central Universities (Grant No.XDJK2010B009).

References

1. Yu G, Gao J, Hummelen J, Wudl F, Heeger A (1995) Science 270: 1789
2. Brabec CJ (2004) Solar Energy Mater Colar Cells 83:273
3. Shoaee S, Clarke TM, Huang C et al. (2010) J Am Chem Soc 132:12919
4. Havinga E, Ten Hoeve W, Wynberg H (1992) Polym Bull 29:119
5. Yang M, Chen X, Zou Y et al. (2013) J Mater Sci 48:3177
6. Negishi E-i, Anastasia L (2003) Chemical reviews 103:1979
7. Zhang W, Tao F, L-y X et al. (2012) J Mater Sci 47:323
8. Li Y (2012) Acc Chem Res 45:723
9. Chochos CL, Avgeropoulos A, Lidorikis E (2013) J Chem Phys 138: 064901
10. Frisch M, Trucks G, Schlegel H et al. (2009) Gaussian 09. Gaussian Inc, Wallingford, CT
11. Shi L-L, Liao Y, Yang G-C, Su Z-M, Zhao S-S (2008) Inorg Chem 47:2347
12. Zou Y, Najari A, Berrouard P et al. (2010) J Am Chem Soc 132:5330
13. Braunecker WA, Oosterhout SD, Owczarczyk ZR et al. (2013) Macromolecules 46:3367
14. Kanal IY, Owens SG, Bechtel JS, Hutchison GR (2013) J Phys Chem Lett 4:1613
15. Seo JH, Jin Y, Brzezinski JZ, Walker B, Nguyen TQ (2009) ChemPhysChem 10:1023
16. Mukaiyama T (1990) Challenges in synthetic organic chemistry. Oxford University Press, Oxford
17. Foster J, Weinhold F (1980) J Am Chem Soc 102:7211
18. Lin BC, Cheng CP, Lao ZPM (2003) J Phys Chem A 107:5241
19. Perdew JP, Burke K, Ernzerhof M (1996) Phys Rev Lett 77:3865
20. Ernzerhof M, Perdew JP (1998) J Chem Phys 109
21. Beaupré S, Pron A, Drouin SH et al. (2012) Macromolecules 45:6906
22. Becke AD (1988) Phys Rev A 38:3098
23. Hoe W-M, Cohen AJ, Handy NC (2001) Chem Phys Lett 341:319
24. Ku J, Lansac Y, Jang YH (2011) J Phys Chem C 115:21508
25. Lan YK, Yang CH, Yang HC (2010) Polym Int 59:16
26. Yang X, Wang L, Wang C, Long W, Shuai Z (2008) Chem Mater 20:3205
27. Zhao Y, Truhlar DG (2006) J Phys Chem A 110:5121
28. Reed AE, Weinstock RB, Weinhold F (1985) J Chem Phys 83:735
29. Klionsky DJ, Abdalla FC, Abeliovich H et al. (2012) Autophagy 8:445
30. Shahid M, McCarthy-Ward T, Labram J et al. (2012) Chem Sci 3:181
31. Chochos CL, Choulis SA (2011) Prog Polym Sci 36:1326
32. Mihailetchi V, Blom P, Hummelen J, Rispens M (2003) J Appl Phys 94:6849
33. Rand BP, Genoe J, Heremans P, Poortmans J (2007) Prog Photovolt Res Appl 15:659
34. Lo M, Ng T, Liu T et al. (2010) Appl Phys Lett 96:113303
35. Scharber MC, Mühlbacher D, Koppe M et al. (2006) Adv Mater 18:789
36. Knupfer M (2003) Appl Phys A 77:623
37. Dennler G, Scharber MC, Ameri T et al. (2008) Adv Mater 20:579
38. Dennler G, Scharber MC, Brabec CJ (2009) Adv Mater 21:1323
39. Yang X, Li Q, Shuai Z (2007) Nanotechnology 18:424029
40. Tao Y, Wang Q, Yang C et al. (2008) Angew Chem 120:8224
41. Chu T-Y, Tsang S-W, Zhou J et al. (2012) Sol Energy Mater Sol Cells 96:155
42. Marcus R, Sutin N (1993) Angew Chem Int Ed Engl 32:1111
43. Deng W-Q, Goddard WA (2004) J Phys Chem B 108:8614
44. Coropceanu V, Cornil J, da Silva Filho DA, Olivier Y, Silbey R, Brédas J-L (2007) Chem Rev 107
45. Kuo MY, Chen HY, Chao I (2007) Chem-A Eur J 13:4750
46. Wang L, Nan G, Yang X, Peng Q, Li Q, Shuai Z (2010) Chem Soc Rev 39:423
47. Marcus RA (1993) Rev Mod Phys 65:599
48. Sun L, Bai FQ, Zhao ZX, Yang BZ, Zhang HX (2010) J Polym Sci B Polym Phys 48:2099
49. Koopmans T (1934) Physica 1:104
50. Lan Y-K, Huang C-I (2008) J Phys Chem B 112:14857